Characterization of a Novel Birnavirus Strain Isolated from Mandarin Fish (*Siniperca chuatsi*)

Hetong Zhang , Dandan Zhou , Junjian Dong , Yunyun Yan , Shanshan Liu , Xing Ye , Jianguo He * , Chengfei Sun *

Posted Date: 17 December 2024

doi: 10.20944/preprints202412.1420.v1

Keywords: Birnavirus; *Birnaviridae*; Mandarin fish; Pathogenicity; Disinfectant

Article

Characterization of a Novel Birnavirus Strain Isolated from Mandarin Fish (*Siniperca chuatsi*)

Hetong Zhang [1,2], Dandan Zhou [3], Junjian Dong [1,2], Yunyun Yan [1,4], Shanshan Liu [5], Xing Ye [1,2], Jianguo He [6,*] and Chengfei Sun [1,2,*]

[1] Key Laboratory of Tropical and Subtropical Fisheries Resource Application and Cultivation, Ministry of Agriculture and Rural Affairs, Pearl River Fisheries Institute, Chinese Academy of Fishery Sciences, Guangzhou 510310, China; zhanght@prfri.ac.cn (H.Z.); dongjj@prfri.ac.cn (J.D.); 20222170546@pgs.hebau.edu.cn (Y.Y.); yexing@prfri.ac.cn (X.Y.)

[2] Key Laboratory of Aquatic Animal Immune Technology of Guangdong Province, Pearl River Fisheries Institute, Chinese Academy of Fishery Sciences, Guangzhou 510310, China

[3] State Key Laboratory of Biocontrol, Southern Marine Sciences and Engineering Guangdong Laboratory (Zhuhai), School of Marine Sciences, Sun Yat-sen University, Guangzhou, China; zhoudd5@mail2.shsu.edu.cn

[4] College of Oceanography, Agriculture University of Hebei, Qinhuangdao 066000, China

[5] School of Ecology, Sun Yat-sen University, Guangzhou 510275, China; liushansh@mail.sysu.edu.cn

[6] School of Life Sciences, Sun Yat-sen University, Guangzhou, China

* Correspondence: lsshjg@mail.sysu.edu.cn (J.H.); scf@prfri.ac.cn (C.S.)

Abstract: Birnaviruses infect a wide range of hosts, including economically important fish species. In this study, we report the isolation and characterization of a novel birnavirus, named mandarin fish birnavirus (MFBV). We obtained the full-length sequence of the MFBV genome. The segment A is 3539 bp, and the segment B is 2719 bp in length. Phylogenetic analyses revealed its close relationship with Largemouth bass birnavirus (LBBV) and Lates calcarifer birnavirus (LCBV) of the Birnaviridae family. Further, characterization of MFBV revealed its rapid replication kinetics that replication cycle is about 8-10 hours in mandarin fish kidney cells. Both intraperitoneal injection and immersion infection routes resulted in severe symptoms in juvenile or fry fish. Mortality was occured within one day post-infection (dpi), with cumulative mortality rates ranging from 41.8% to 83.6% depending on the challenge method. Notably, compared to juvenile fish, fry fish exhibited higher susceptibility to infection. Viral RNA copies in multiple tissues ranged from the highest of $10^{7.9}$ to the lowest of $10^{6.9}$ per μg total RNA revealed that MFBV has a broad tissue tropism. Histopathological examination showed characteristic lesions, including villus damage in the intestine, necrosis in the spleen and kidney cells. MFBV was most sensitive to glutaraldehyde, with a final concentration of 20 ppm resulting in an 8 log-unit reduction in titer. While povidone-iodine, formaldehyde, sodium hypochlorite, hydrogen peroxide, and potassium permanganate required concentrations in the 10^3 ppm range to achieve similar efficacy. The half-life of the virus during different phase was 36.5 hours to 144.5 hours.

Keywords: Birnavirus; *Birnaviridae*; mandarin fish; pathogenicity; disinfectant

1. Introduction

The family *Birnaviridae* includes seven genera. Among these, the *Aquabirnavirus*, *Avibirnavirus* and *Blosnavirus* infect vertebrates, while the remaining genera, *Dronavirus*, *Entomobirnavirus*, *Ronavirus* and *Telnavirus* infect insects, rotifers, or mollusks (International Committee on Taxonomy of Viruses, Virus Taxonomy: 2023 Release). Notably, infectious pancreatic necrosis virus (IPNV, genus *Aquabirnavirus*) and infectious bursal disease virus (IBDV, genus *Avibirnavirus*) are extensively studied birnaviruses that primarily affect salmonids and poultry, respectively.

Birnaviruses have bisegmented double-stranded RNA (dsRNA) genomes with a total of about 6 kbp. Segment A, approximately 3.1-3.5 kbp in length, encodes a polyprotein of VP2- (X)-VP4-VP3. The segment B, around 2.7 kbp in length, encodes the viral RNA-dependent RNA polymerase (RdRp,

 doi:10.20944/preprints202412.1420.v1

VP1). The polyprotein undergoes autocatalytic cleavage by the VP4 protease, yielding in precursor VP2 (preVP2), VP4, and VP3. The preVP2 is subsequently matured by cleaving the C-terminal small peptides and then matured VP2 constitutes the capsid. While VP3 is a ribonucleoprotein [1,2].

Birnaviruses are non-enveloped, single-layered capsid dsRNA viruses, distinct from the double-layered capsid of most dsRNA viruses. Their capsid is icosahedron, clustered as 260 outer trimers, arranged with a triangulation number of T=13, and has a diameter of approximately 60-70nm, as observed in representative birnaviruses such as IBDV and IPNV [3,4].

In recent years, two novel fish birnaviruses, namely largemouth bass birnavirus (LBBV) reported in 2022 and Lates calcarifer birnavirus (LCBV) identified in 2019, have been described. LBBV has been associated with high virulence results in massive mortality in largemouth bass (*Micropterus salmoides*), whereas LCBV infection has only been linked to mild clinical signs in seabass (*Lates calcarifer*) [5,6]. These findings suggested that birnaviruses may have become prevalent in farmed fish in southeast Asia in recent years. Although several novel birnavirus genomes have been sequenced in recent years [5–7], there is still a lack of updated information on the gene structure of the Birnaviridae family.

In this study, we isolated a highly pathogenic birnavirus from mandarin fish, an economically important fish species in southern China. We obtained the complete genome of this virus and characterized its replication dynamics and virulence. We also conducted a detailed analysis of the genome structure of MFBV and other birnaviruses. The inactivation efficiency of the disinfectant on MFBV was also tested.

2. Materials and Methods

2.1. Animals and Cells

Healthy juvenile mandarin fish weighing 10 ± 2 g and fry mandarin fish weighing 0.02 g were obtained from Foshan, Guangdong Province, China. The *Siniperca chuatsi* kidney cell (SCK) were isolated and maintained in our laboratory [8].

2.2. Isolation of the Viral Strain

In the original case, part of mandarin fish (weighing 15-20 g) in the pond can be seen floating on the water and dead within a few hours. Spleen and kidney tissues from cases were underwent sampling. Ten times the volume of PBS was added, and the tissues were thoroughly homogenized. The homogenate was filtered through a 0.45 μm filter (Millipore, USA) to remove bacterial contamination, and then inoculated into SCK cells at a ratio of 1:100 (v/v) and incubated at 27 °C. Cytopathic effect (CPE)-positive cells were identified using phase-contrast microscopy. Infected cells underwent three freeze-thaw cycles and were vortexed for 10 seconds to homogenize. The yielded virus was regarded as the first passage virus. Following subsequent rounds of infection in SCK cells, the viral progeny generated is sequentially referred to as the second passage, third passage, and so forth. Viral culture medium was harvested as the virus stock and stored at −80 °C. The isolated virus strain was designated as MFBV-22TIE (Accession:PP786692.1; PP786693.1).

2.3. Library Construction, Sequencing, and Genome Assembly

Extracting RNA from MFBV-infected SCK cells, and then RNA library was constructed by using the RNA library prep kit for Illumina (New England Biolabs, Ipswich, MA, USA) according to the manufacturer's protocol. The library was sequenced on the Illumina NovaSeq platform (Illumina, USA) at Majorbio (Shanghai, China), generating 150-bp paired-end reads. The raw sequencing reads were filtered and quality-trimmed using fastp (version 0.21.0) to remove low-quality bases and adapters. The resulting high-quality reads were de novo assembled using SPAdes (v3.15.4) in metagenomic mode ('-meta') with default settings. Contigs longer than 1000 bp were annotated against the NCBI nonredundant protein (nr) database using DIAMOND (blastx, version 2.0.11) with a stringent E value of 1E-5 to eliminate false-positive results.

 doi:10.20944/preprints202412.1420.v1

2.4. Amplification of Genome Terminal Sequence

Viral RNA was extracted from MFBV-infected cell cultures using a Monarch Total RNA Miniprep Kit (New England Biolabs). Poly (A) tailing of viral genome RNA using E. coli Poly (A) polymerase (New England Biolabs). The SMARTer RACE kit (Takara, Japan) was employed to amplify the terminal sequences of genome. First-strand cDNA synthesis was performed using a modified oligo (dT) primer with an adapter sequence at the 5' end. The 5' and 3' ends of the cDNA were then amplified using nested specific primers of and the universal primer mix provided in the kit. The amplified products were analyzed by gel electrophoresis, and bands of interest were purified and sequenced using Sanger sequencing technology. The obtained sequences were then assembled and analyzed to determine the terminal sequences of the RNA virus genome. The specific primers used are list below:

SegmentA-3'-outer	CCCTCACCCAGAGGAGCACCAAACT
SegmentA-3'-inner	CAAGCCCCTGCACCACCAGAGTTTG
SegmentA-5'-outer	CGGAGAGTACCCTGCTGACCAGTCT
SegmentA-5'-inner	AGGCCTTCTTCAGGTCCTGTGAGGT
SegmentB-3'-outer	AAAGAAGCAGAAGCAGCAGCCGACC
SegmentB-3'-inner	ACCGACGACTGGGGAGAAGCATCAG
SegmentB-5'-outer	GCTCGGGCTTGTGCATGGGGTAGTA
SegmentB-5'-inner	CGACGAGTACAGCCAGACTGGGGAG

2.5. Analysis of the MFBV Genome

Phylogenetic trees were constructed using MEGA (Version 4.0) software by maximum likelihood method with default parameters. Multiple sequence alignment was performed using Kalign [9]. The birnavirus sequences used in phylogenetic analysis were: Largemouth bass birnavirus (LBBV), MW727622.1 and MW727622.1; Lates calcarifer birnavirus (LCBV), MK103419.1 and MK103420.1; Blotched snakehead virus (BSNV), AJ459382.1 and AJ459383.1; Infectious pancreatic necrosis virus (IPNV), AJ622822.1 and AJ622823.1; Infectious bursal disease virus (IBDV), MZ888508.1 and MZ888507.1; Drosophila melanogaster birnavirus (DBV), GQ342962.1 and GQ342963.1; Rotifer birnavirus (RBV), FM995220.1 and FM995221.1; Tellina virus 1 (TV-1), AJ920335.1 and AJ920336.1; Drosophila x virus (DXV, U60650.1 and NC_004169.1.

2.6. Assessment of Cytopathic Effect

SCK cells were employed to assess the CPE induced by MFBV. Cells were passaged at an appropriate ratio, in triplicate, in 25 cm^2 flasks to ensure a confluent monolayer, and then infected with MFBV. The initial infectious dose was established at a multiplicity of infection (MOI) of 3. Phase-contrast images were captured using a ZEISS Observer.Z1 inverted microscope at indicated time points.

2.7. Transmission Electron Microscopy

SCK cells were inoculated with MFBV at an MOI of 5. At 16 hours post-infection (hpi), cells were gently scraped, centrifuged at 500× g for 3 minutes, and then fixed using 2.5% glutaraldehyde. Following osmium tetroxide post fixation, uranyl acetate was applied to enhance membrane contrast. Epoxy resin served as the embedding medium. The ultrathin sections were visualized using a Hitachi HT7800 transmission electron microscope.

The fish spleen and kidney tissues were cut into 1 mm^3 pieces and fixed in 2.5% glutaraldehyde. Secondary fixation was performed with osmium tetroxide. The fixed specimens were dehydrated by incubation in a series of ethanol solutions (30%, 50%, 70%, 80%, 95%, and 100%) followed by 100% acetone. After resin infiltration and embedding, the samples were sectioned to 80 nm thickness, mounted on copper mesh, and post-stained with lead citrate. The ultrathin sections were visualized using a Hitachi HT7800 transmission electron microscope.

 doi:10.20944/preprints202412.1420.v1

2.8. Virus Titer Assays

SCK cells were seeded in 48-well plates with 200 μl of medium in each well. The 3rd-passage MFBV samples collected at indicated time points underwent 3 freeze-thaw cycles and were vortexed for 10 s for homogenization. Samples were then titrated using 10-fold serial dilutions, with six wells being inoculated with 200 μl of each dilution. Wells were designated as positive if typical CPE was observed at 7 dpi. The 50% tissue culture infective dose ($TCID_{50}$) values were computed using the $TCID_{50}$ calculator (Marco binder, University of Heidelberg, Heidelberg, Germany) based on the Spearman–Kärber method [10]. Virus titer values represent mean ± SE for three biological replicates of MFBV samples.

2.9. Artificial Challenge

In juvenile mandarin fish intraperitoneal injection challenge study, groups of 15 fish were kept in 150 L tanks at temperatures ranging from 28 to 30 °C. Each fish received an intraperitoneal injection of 10^9 $TCID_{50}$ 3rd-passage MFBV suspended in 0.2 ml cell culture medium. Additionally, ten fish were administered the same volume of untreated cell cultures to serve as controls. Fish mortality was monitored daily for three weeks, with cumulative mortality data collated from the three separate experiments.

In the juvenile and fry mandarin fish immersion challenge study, fish were immersed in water with a virus concentration of 10^7 $TCID_{50}$/ml for 20 minutes, then transferred to 150 L tanks at 28 to 30 °C. For fry fish, the study concluded on 3 dpi.

2.10. Absolute Quantitative RT-PCR

Nine fish were sampled per treatment group, 14 tissues and intestinal content samples were collected at 16 hpi, including spleen, pronephros, mesonephros, metanephros, pyloric caeca, intestine, intestinal contents, stomach, thymus, heart, skin, gill, liver, gonad and brain. RNA of samples were isolated using a Monarch Total RNA Miniprep Kit. RNA was incubated at 65 °C for 5 minutes and promptly placed on ice to denature RNA double strands and secondary structures. Reverse transcription was performed using Induro Reverse Transcriptase (New England Biolabs) according to the manufacturer's protocol.

Absolute quantitative PCR with primers for MFBV segment A was performed (Applied Biosystems 7300 Real-Time PCR System) to quantify the total copies of viral genome and mRNA. The standard samples consist of a series of tenfold dilutions of segment A PCR amplification products with known concentrations. RT-qPCR was performed in a total reaction volume of 20 μl containing 0.2 μM primers, 1 μl of cDNA, 10 μl of 2 × SYBR Green Premix (Takara, Japan), and 7.2 μl of RNase-free water. The following settings were used: 40 cycles of amplification for 10 seconds at 95 °C and 30 seconds at 65 °C. Each sample was run in technical triplicates. Primers used were: MFBVsegA-qPCR-F: CTGGATAGCCAGGAACGACC; MFBVsegA-qPCR-R: GTTGTCGGCGTACACTTCCT

2.11. Histopathological Sectioning and H&E Staining

Intestine, spleen and metanephros tissues were fixed with formalin and acetic acid fixative overnight, and preserved with 70% ethanol. Dehydration was sequentially performed using 70%, 80%, 95%, and anhydrous ethanol. Then, these samples were embedded in paraffin and sectioned. The slices were stained with hematoxylin-eosin (H&E) and prepared as permanent slides after they were dried, dewaxed, and hydrated. The slices were then observed under the microscope.

2.12. Determine the Inactivation Efficiency of Disinfectants

All disinfectants were diluted to the appropriate concentrations using sterile ultrapure water and added to the virus suspension (11 Log^{10} $TCID_{50}$/ml). The mixture was immediately vortexed for 10 seconds for homogenization and centrifuged at 100 × g for 3 seconds to collect the liquid from the tube lid. After incubation at 25°C for 30 minutes, the viral titer was immediately assayed using the

 doi:10.20944/preprints202412.1420.v1

method described above. The cells were incubated with the same concentration of disinfectant as a control to exclude the effect on cell activity by disinfectant.

2.13. Determination of the Stability of MFBV Suspension

MFBV infected SCK cell culture (at 24 hours post infection with a titer of 11.73 Log^{10} $TCID_{50}$/ml) was incubated for up to 90 days at room temperature and dark conditions, and tested for its infectivity. Briefly, at desired time-points, the inoculated objects were vortexed for 3 seconds to homogenize the precipitate and retrieved, then immediately assayed titers in SCK cells using the method described above.

3. Results

3.1. Tissue Electron Microscopy

In July 2022, a fish farm in Nansha District, Guangzhou, experienced persistent death of mandarin fish, with a cumulative mortality rate reaching 80% after three weeks. Subsequent bacterial tests and infectious spleen and kidney necrosis virus (ISKNV), Mandarin fish ranavirus (MRV), Siniperca chuatsi rhabdovirus (SCRV), and nervous necrosis virus (NNV) screenings were all negative. Spleen and kidney samples from the dead fish were collected for transmission electron microscopy (TEM). Virus-like particles with diameters of approximately 60–80 nm observed in both tissues, with some displaying a polyhedral morphology (Figure 1).

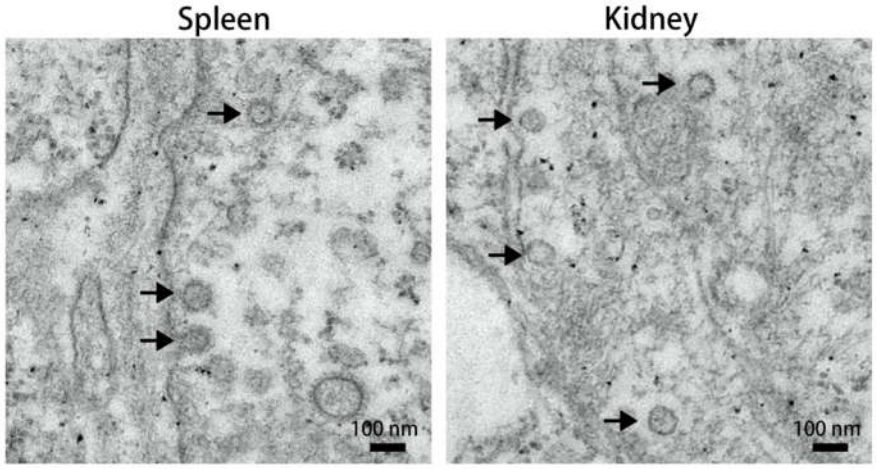

Figure 1. TEM micrographs of spleen and kidney tissue from the dead fish. Arrows indicate virus-like particles with a polyhedral morphology.

3.2. Assessment of Cytopathic Effect

Upon inoculation with tissue homogenization, highly refractive regions appeared at the edges of cells at 5.5 hpi, indicating morphological and/or refractive index changes in infected cells. By 8.5 hpi, obviously CPE manifested, characterized by cell rounding and detachment from the substrate, and the number of CPE cells peaked at 20 hpi. Subsequent passages of the viral culture fluid to fresh SCK cell monolayers showed a similar pattern of CPE. In contrast, the control SCK cell monolayer remained normal and intact throughout the incubation period (Figure 2).

 doi:10.20944/preprints202412.1420.v1

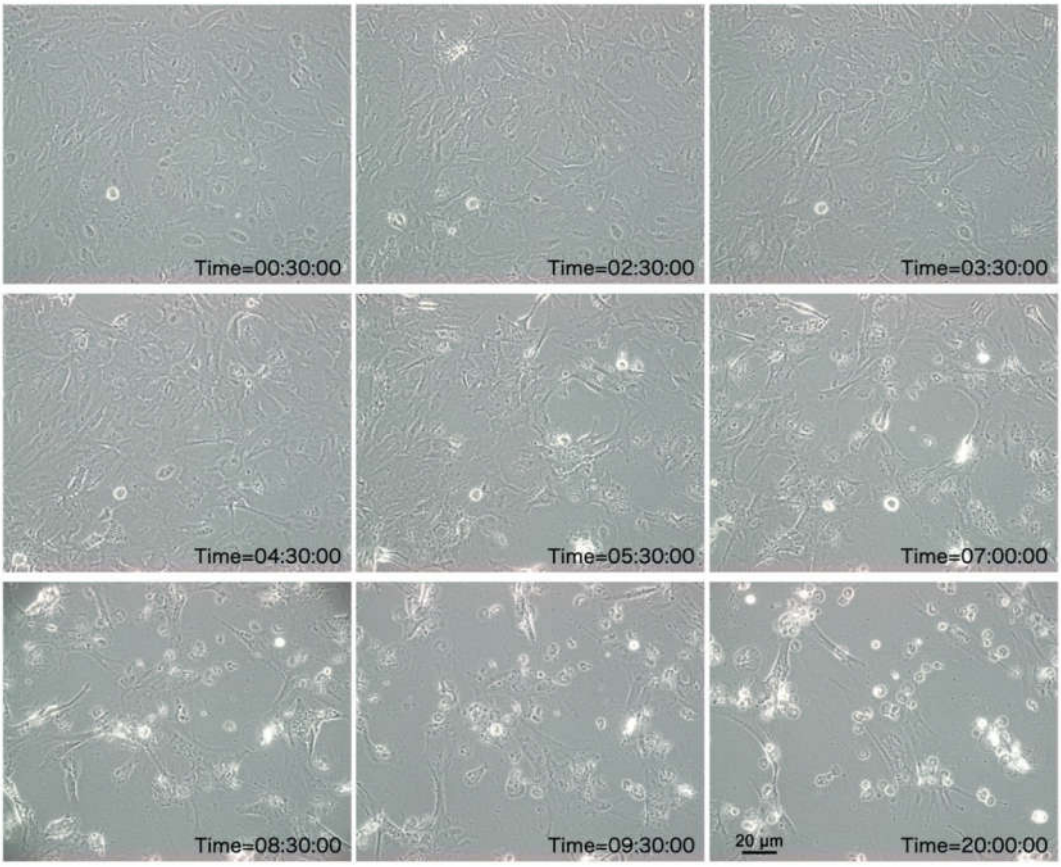

Figure 2. Phase contrast microscopic images depicting CPE in SCK cells elicited by the 3rd passage of MFBV at different hpi. All images were obtained within the same field of view.

3.3. Transmission Electron Microscopy Observation

Further, we observed virions in the cytoplasm of MFBV-infected SCK cells using transmission electron microscopy. The diameter of virus particles, measured from different symmetry axes, ranged from 65 nm to 80 nm. These particles exhibited an icosahedral capsid with an electron-dense core. Upon examination at higher magnification, the particles displayed a rough surface structure (Figure 3).

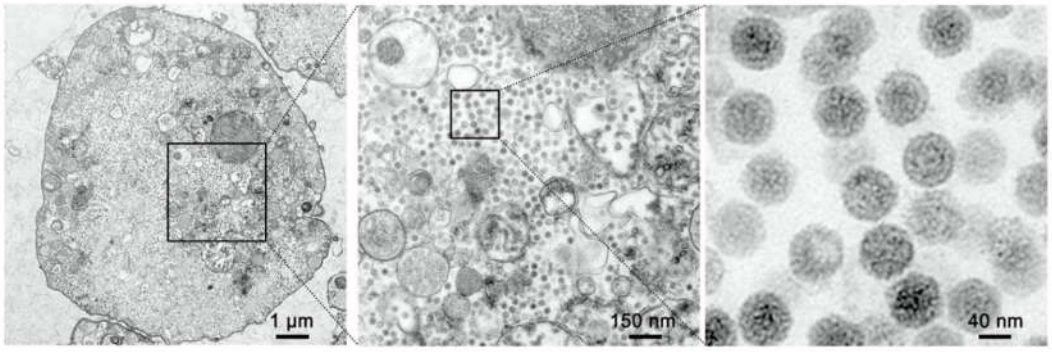

Figure 3. TEM micrographs of MFBV-infected SCK cells. The images on the right side are magnified views from the boxed region in adjacent left images.

3.4. The Organization of MFBV Genome

The MFBV genome was obtained through high-throughput sequencing and rapid amplification of cDNA ends (RACE) methods. The length of MFBV segment A is 3539 bp, and segment B is 2719

 doi:10.20944/preprints202412.1420.v1

bp, with GC contents of 57.33% and 56.34%, respectively. The open reading frames (ORFs) were delineated by homology aligning with reference sequences of IPNV [11], IBDV [12] and BSNV [13], which have been experimentally validated. MFBV segment A, encoding a polyprotein of 5'-preVP2-X-VP4-VP3-3' from 171 bp to 3443 bp, while segment B encodes VP1 from 97 bp to 2667 bp. Overall, the genetic organization of MFBV is similar to that of other birnaviruses, albeit with a several distinct exceptions. Firstly, MFBV was distinguished by the presence of X gene, a feature shared only with a subset of birnaviruses, including LCBV, BSHV and TV-1 (Figure 4). The specific function of the X gene remains unknown [13], but its presence contributed to a longer length of MFBV segment A compared to other birnaviruses. Secondly, MFBV lacked an overlapping gene named small ORF or VP5, which is approximately 400 bp in length and is present in most birnaviruses, with exception of LBBV and RBV [14]. Notably, the VP5 corresponding to the small ORF has been confirmed to be expressed in IPNV and IBDV [15,16], but its sequences are non-homologous and its genomic location is irregular. For example, the small ORF in DXV is located between VP4 and VP3 [17], whereas in DBV it was located within VP2 [18] (Figure 4). Thirdly, three small peptides are predicted to be cleaved from MFBV preVP2 during the maturation process, with lengths of 43 aa, 7 aa, and 18 aa. This differs from the four peptides found in BSNV and IBDV (Figure 4). These small peptides are recognized as capsid-associated peptides and have biological functions of deforming and perforating biological membranes [19,20].

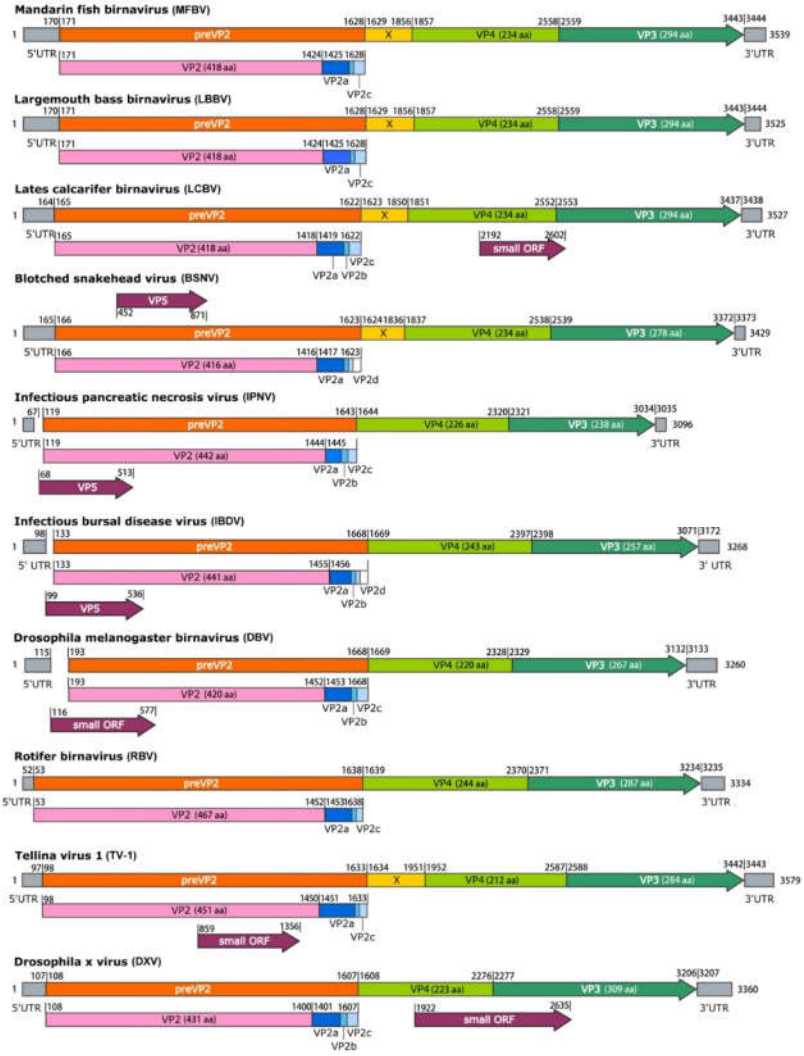

Figure 4. Schematic representation of the segment A genome organization of MFBV and other representative birnaviruses. The additional pink graphics illustrating processing of preVP2.

 doi:10.20944/preprints202412.1420.v1

Polyprotein cleavage sites are indicated by vertical bars and identified by nucleotide positions. Numbers at the 3′-ends indicate the full length of segment A.

Phylogenetic analysis of polyprotein and VP1 was conducted using maximum likelihood on the amino acid level, incorporating representatives from seven genera in the *Birnaviridae* family. Additionally, percent identity matrices were generated for the four proteins to examine their identity. The results showed that both the polyproteins and VP1 of MFBV, LBBV, and LCBV clustered into a single evolutionary branch, with the four mature proteins displaying 95.92% to 99.57% sequence homology. Furthermore, whatever the protein analyzed, MFBV appears to be phylogenetically distant from other birnaviruses. Among other branches, the genetically closest virus was BSNV, another fish birnavirus, with VP2, VP4, VP3, and VP1 showing sequence homologies of only 55.93%, 43.03%, 46.72%, and 61.36%, respectively. While IPNV exhibited even lower homologies, ranging from only 25% to 48.94% (Figure 5). In these four proteins, VP2 and VP1 are relatively conserved, attributed to their requirement for conserved folding and topological structure [21]. Conversely, VP4 and VP3 have diverged significantly during birnavirus evolution, exemplified by the mere 20% sequence homology between MFBV and DXV (Figure 5).

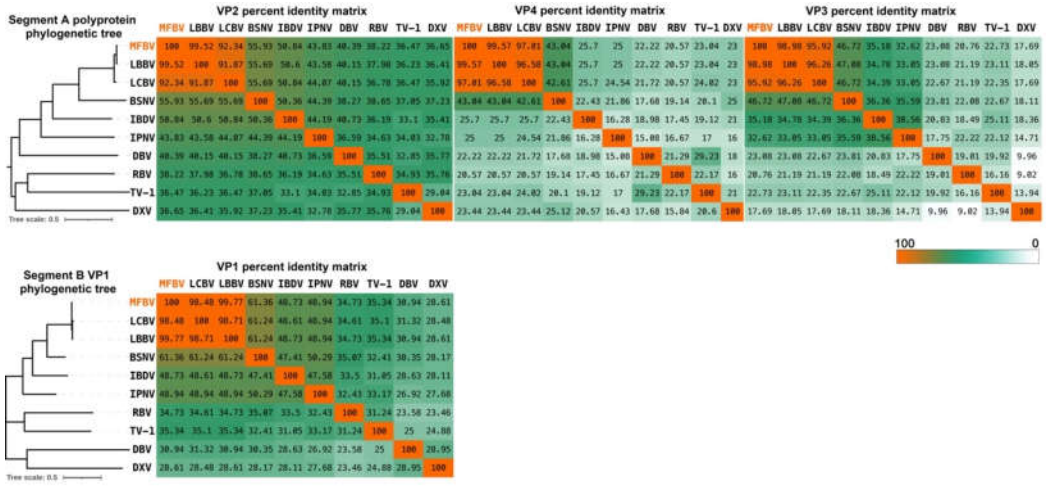

Figure 5. Distance tree representing the phylogenetic relationships of the polyprotein and VP1 within the *Birnaviridae* family. The percent identity matrices are generated based on VP2, VP3, VP4 and VP1 amino acid sequences.

3.5. Virus Titer Assays

To investigate the infectious dynamics of MFBV, we harvested the 3rd passage virus cell culture at various time points post-infection. We then inoculated this viral fluid into SCK cells obtaining viral titers. The results revealed a rapid increase in viral titers from 8 to 10 hpi, rising from $10^{7.2}$ to $10^{9.2}$ $TCID_{50}$/ml. By 20 hpi, the titers had reached $10^{11.4}$ $TCID_{50}$/ml and remained stable near peak levels up to 48 hpi. These findings suggest that a single cycle of replication for MFBV takes approximately 8–10 hours (Figure 6).

 doi:10.20944/preprints202412.1420.v1

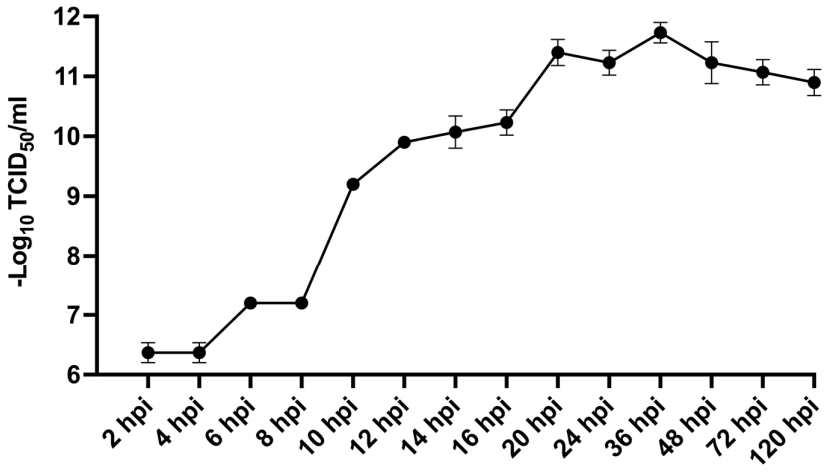

Figure 6. Infectious dynamics of MFBV in SCK cells. Viral titers of the 3rd passage of MFBV at indicated time points were measured and expressed as $TCID_{50}$/ml. Each titer value represents the mean ± SE derived from three biological replicates. Partial SE is hidden within the data points.

3.6. MFBV Artificial Challenge

The virulence of the 3rd-passage MFBV from SCK cell was evaluated in juvenile (~10 grams of body weight) and fry (~0.02 grams of body weight) mandarin fish. Prior to the challenge, viscera from three juvenile and fry fish were sampled and examined for the absence of ISKNV, MRV, SCRV and MFBV by PCR. Juvenile mandarin fish were then subjected to intraperitoneal injection and immersion challenges. In the intraperitoneal injection challenge study, mortality induced by MFBV began at 6 hpi, rapidly escalating to 62.9% by 12 hpi, and reaching 74.7% at 24 hpi, then persisting throughout the subsequent 14-day observation period. No mortality was observed among the control fish (Figure 7A). In the immersion challenge, mortality was initially observed between 12-24 hpi, reaching 37.5% at 36 hpi, and further increasing to 41.8% at 48 hpi, then ceasing throughout the observation period. No mortality was observed among the control fish (Figure 7B). Both challenge methods led to similar clinical manifestations, including congestion of the head skin, visceral congestion, ascites containing red blood cells comprising 2%-5% of body weight, and intestines filled with jelly-like mucus (Figure 7D–I). In the bath challenge of fry fish, mortality rapidly increased during 6-24 hpi, reaching 83.6% by 48 hpi. However, at 48 hpi, the control group also exhibited a modest mortality of 19.9%. Consequently, the estimated corrected mortality in fry fish caused by MFBV ranged roughly between 63.7% to 83.6% (Figure 7C). In the immersion experiment with the same titer, the virulence of MFBV to fry was higher than that to juvenile fish. Furthermore, the viscera homogenates of deceased fish tested positive for MFBV by RT-qPCR, while those of control fish tested negative. When inoculated with the homogenates from cases, SCK cell cultures developed characteristic cytopathic effects. These results collectively demonstrate the pathogenicity of MFBV to both juvenile and fry mandarin fish.

 doi:10.20944/preprints202412.1420.v1

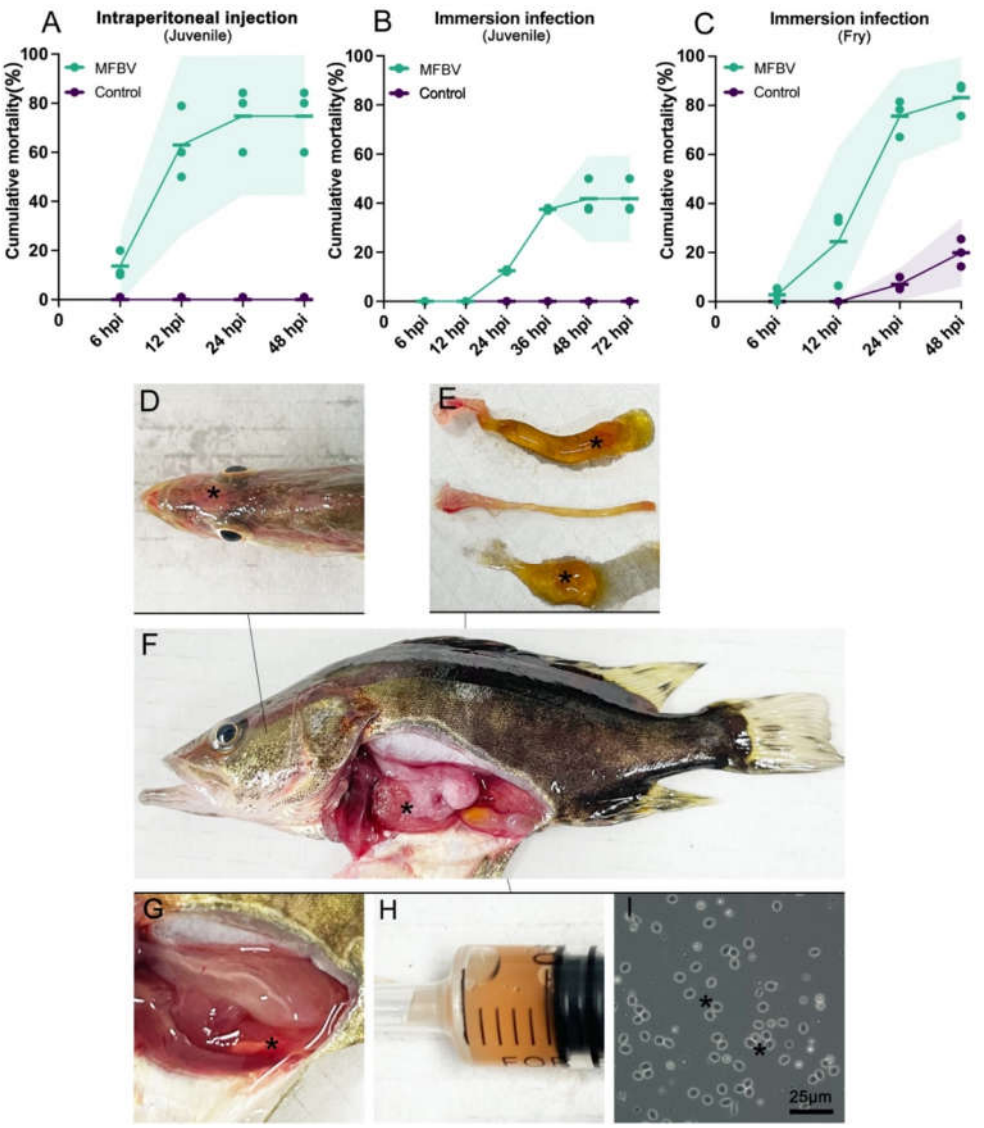

Figure 7. (A–C) The cumulative mortality rates in MFBV-infected mandarin fish; mean ± SD from three independent experiments, with the shadow representing the 95% confidence interval. (A) Juvenile mandarin fish as the experimental subjects, challenged via intraperitoneal injection. (B) Juvenile mandarin fish as the experimental subjects, challenged via immersion. (C) Fry mandarin fish as the experimental subjects, challenged via immersion. (D–I) Symptoms of MFBV-infected mandarin fish. (D) Congestion of the head skin (denoted by asterisks) (E) From top to bottom, the intestine filled with mucus, the intestine after removing the mucus, and the mucus itself. Asterisks indicate the yellow mucus. (F) Anatomical view of MFBV-infected mandarin fish. Asterisks indicate visceral congestion. (G–H) Asterisks indicate pale red ascites. All ascites (~0.5 ml) account for approximately 5% of body weight. (I) Asterisks indicate red blood cells observed in the ascitic fluid smear.

3.7. Tissue Distribution of MFBV

We further measured the total copy number of MFBV segment A genomic and messenger RNA in 14 tissues and intestinal content from nine infected juvenile fish using RT-qPCR. The highest viral RNA copy number was observed in the spleen tissue, with an average of $10^{7.94}$ viral RNA copies per μg of total RNA. Additionally, the three kidney organs, including pronephros, mesonephros, and metanephros, also exhibited high levels of viral RNA, ranging from $10^{7.72}$ to $10^{7.83}$ copies. In the digestive systems, the intestine and pyloric caeca showed approximately $10^{7.44}$ copies. For skin, heart,

 doi:10.20944/preprints202412.1420.v1

gill and thymus tissue, the copy numbers reached $10^{7.40}$, $10^{7.34}$, $10^{7.29}$ and $10^{7.19}$, respectively. Other tissues, such as the stomach, liver, gonad, brain, and intestinal contents, showed lower concentrations of approximately $10^{6.9}$ RNA copies per μg total RNA (Figure 8). These results indicate that during intraperitoneal infection, MFBV can infect multiple organs throughout the body, with the highest copy numbers in the spleen and kidneys.

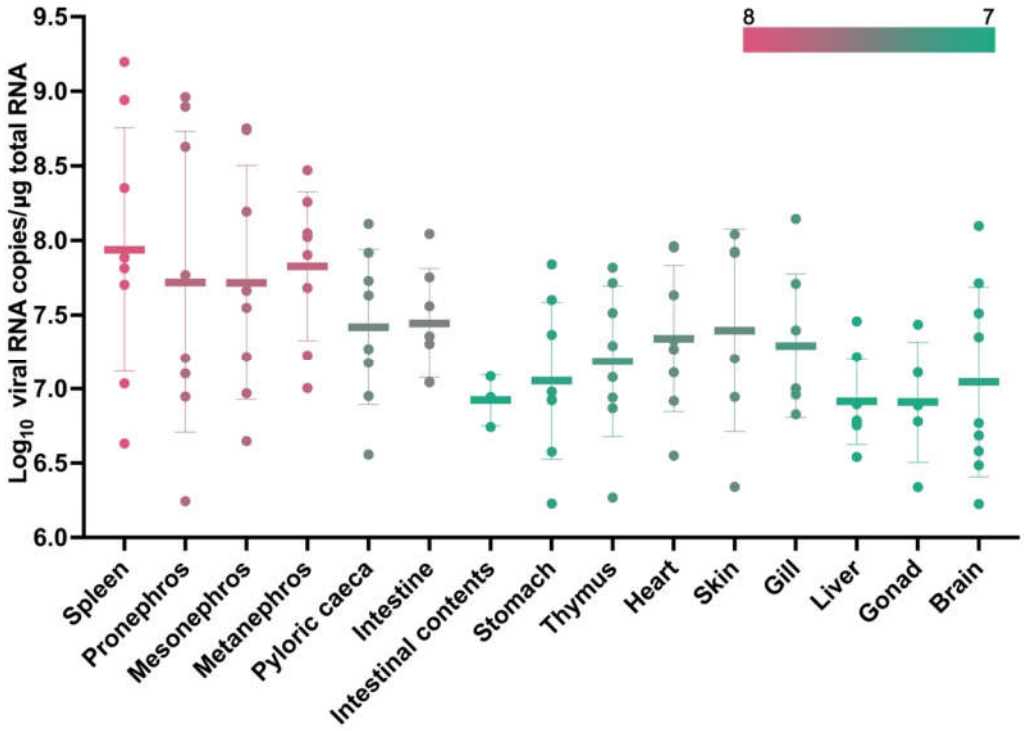

Figure 8. RT-qPCR measured the copy number of MFBV segment A RNA in 14 tissues and intestinal content of MFBV-infected mandarin fish. The color scale indicates the level of viral copy numbers. Mean ± SD from tissues of nine fish.

3.8. Histopathology

In intestine tissue sections infected with MFBV, evident damage to villus structures was observed, characterized by shedding of the simple columnar epithelium layer and rupture of goblet cells, leading to exposure of the lamina propria to the intestinal lumen (Figure 9A,C). In contrast, healthy intestinal villi displayed a dense layer of simple columnar epithelial cells on the surface, along with clearly distinguishable goblet cell vacuoles (Figure 9B,D). Tissue section observation also revealed varying degrees of chromatin condensation in some spleen cells, along with instances of nuclear loss and vague cellular outlines (Figure 9E, G1-G4). In addition, several areas had a loss structure detail (Figure 9G). The abnormal cell morphology, indicative of pyknosis and karyolysis, was widely recognized in MFBV-infected spleen tissue indicated cell death, but not observed in control tissues (Figure 9E–H). Furthermore, in MFBV-infected kidney tissue, red blood cell infiltration was observed around the arteries, whereas in control sections, blood cells, including red blood cells, were contained within the arteries. However, no structural damage on the arteries was observed, the source of the leaked red blood cells could not be conclusively determined from the slices (Figure 9I–L). Additionally, a group of cells with chromatin condensation and larger intercellular spaces aggregated into clusters and displayed multifocal distribution in MFBV infected kidney tissue. Conversely, these features were not observed in the control kidney tissue (Figure 9I–L). These pieces of evidence suggest that MFBV-infection results in damage to multiple visceral organs.

 doi:10.20944/preprints202412.1420.v1

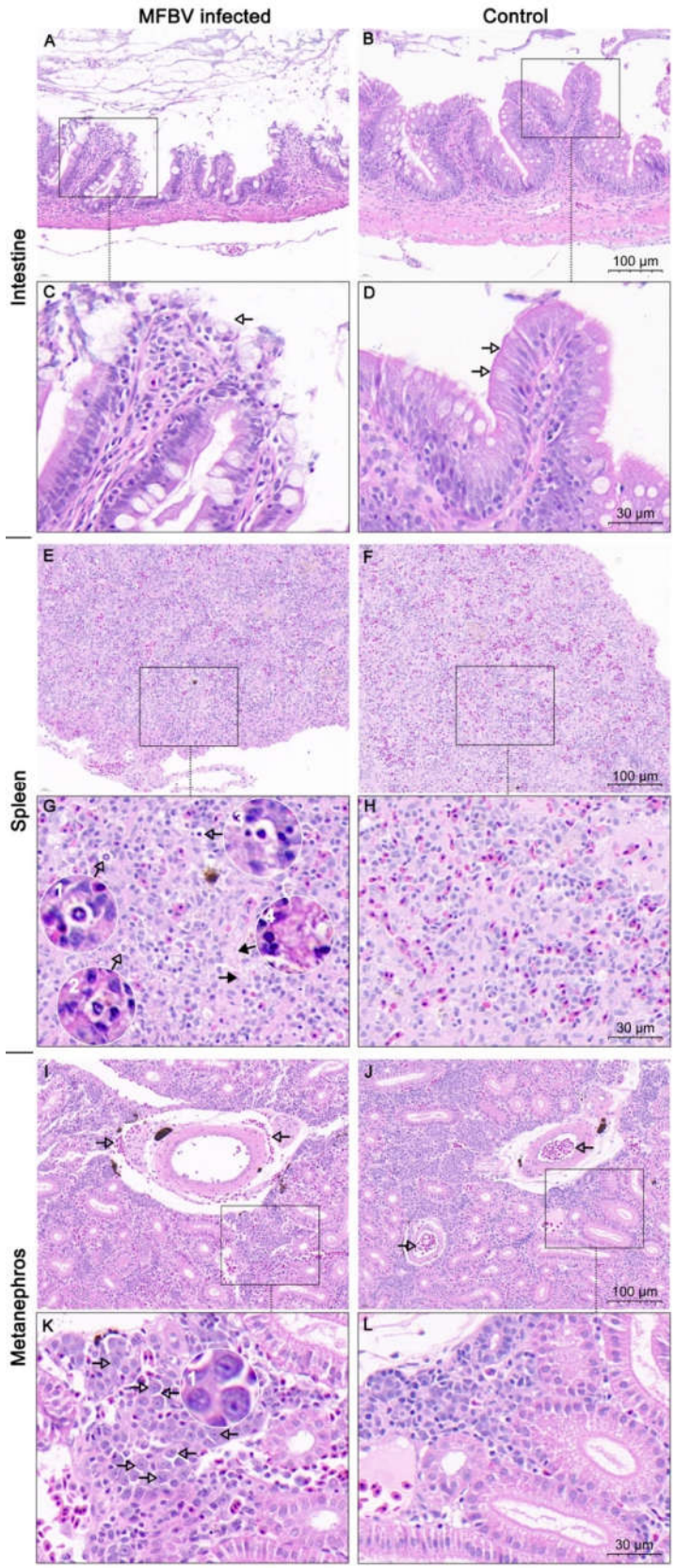

Figure 9. H&E staining analysis of MFBV-infected or healthy mandarin fish tissue sections. (A,C) Intestinal tissue of MFBV-infected mandarin fish, where arrows indicate damage to the simple columnar epithelium layer and rupture of goblet cells. (B,D) Intestinal tissue of control mandarin fish,

 doi:10.20944/preprints202412.1420.v1

displaying a complete mucosal layer, simple columnar epithelial cell layer, and visible goblet cell vacuoles. (E,G) Spleen tissue of MFBV-infected mandarin fish. The hollow arrow and magnified view (G1–G3) indicate nuclear condensation (pyknosis), while the solid arrow and image (G4) show nuclear loss and vague cellular outlines (karyolysis and cell death) and the areas that loss structure detail. (F,H) Control mandarin fish spleen tissue. (I,K) Arrows in (I) indicate red blood cells surrounding the artery. Arrows in (K) and magnified view (K1) indicate abnormal chromatin condensation. (J,L) Control kidney tissue, where blood cells are contained within the arteries (arrow) and nuclei morphology appears normal.

3.9. Efficacy of Disinfectants at Inactivating MFBV

MFBV virus suspension was treated with various disinfectants at different final concentrations for 30 minutes, followed by viral titer determination using the limiting dilution method. The results showed that aldehyde-based disinfectants have strong inactivation efficacy against MFBV, with glutaraldehyde being the most effective. A concentration of 20 ppm glutaraldehyde reduced the titer by 8 Log^{10} $TCID_{50}$, whereas formaldehyde achieved the same reduction need 2000 ppm final concentrations (Figure 10). Povidone-iodine, an iodine-based disinfectant, reduced the titer by 4 Log^{10} $TCID_{50}$ at 2000 ppm, and 20000 ppm resulted in an 8 Log^{10} $TCID_{50}$ reduction. For benzalkonium bromide, 600 ppm reduced the titer by 4 Log^{10} $TCID_{50}$, 6000 ppm by 7 Log^{10} $TCID_{50}$, and 60000 ppm by 8 Log^{10} $TCID_{50}$. Oxidizing agents such as sodium hypochlorite reduced the titer by 4 Log^{10} $TCID_{50}$ at 100 ppm, 5 Log^{10} $TCID_{50}$ at 1000 ppm, and 8 Log^{10} $TCID_{50}$ at 10000 ppm. Hydrogen peroxide reduced the titer by 4 Log^{10} $TCID_{50}$ at 6000 ppm and 8 Log^{10} $TCID_{50}$ at 20000 ppm, while potassium permanganate achieved a reduction of 5 Log^{10} $TCID_{50}$ at 2000 ppm and 8 Log^{10} $TCID_{50}$ at 20000 ppm. Overall, glutaraldehyde and benzalkonium bromide achieved disinfection efficacy of over 3 log-unit need concentrations at the 10^2 ppm range. While povidone-iodine, formaldehyde, sodium hypochlorite, hydrogen peroxide, and potassium permanganate required concentrations in the 10^3 ppm range to achieve similar efficacy. Notably, ethanol showed no inactivation effect on MFBV at concentrations of 25%, 50%, and 75%.

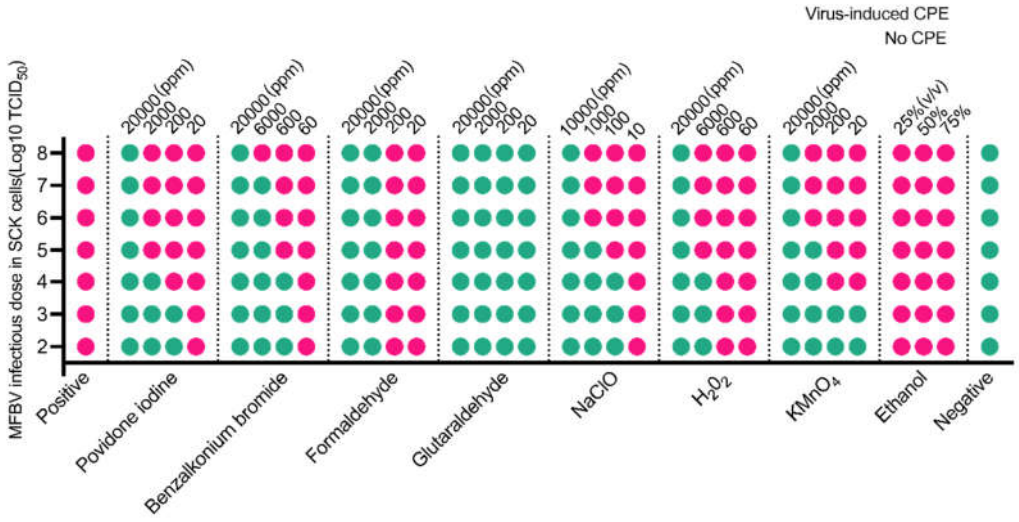

Figure 10. Titer determination of disinfectants treated MFBV virus suspension within SCK cells. Virus-induced CPE positivity is indicated by pink dots, while negativity is indicated by green dots. The data were obtained from three biological replicates, and the results were consistent across experiments.

3.10. Stability of MFBV

MFBV-infected SCK cells suspension was collected at 2 dpi and incubated for up to another 90 days to monitor the titer decay. The initial viral titer was 11.73 Log^{10} $TCID_{50}$/ml, and by the end of the

 doi:10.20944/preprints202412.1420.v1

experiment on day 90 at room temperature, the titer had decreased to 4.2 Log^{10} $TCID_{50}$/ml (Figure 11). Since the sampling timeline was not evenly spaced, the data were split into two segments to analyze. Using data from days 0, 5, 10, and 15 as segment 1, we calculated that it took approximately 15.2 days for the titer to decrease by 3 log-unit, corresponding to a 99.9% reduction in infectious viral particles. The half-life of the virus during this phase was 36.5 hours. Using data from days 30, 60, and 90 days as segment 2, the time required for the logarithm of the titers to halve (5.86 log-unit) was calculated to be 52.8 days, with a viral half-life of 144.5 hours during this phase. The half-life of MFBV seems to show biphasic decay of short half-life and long half-life at different stages.

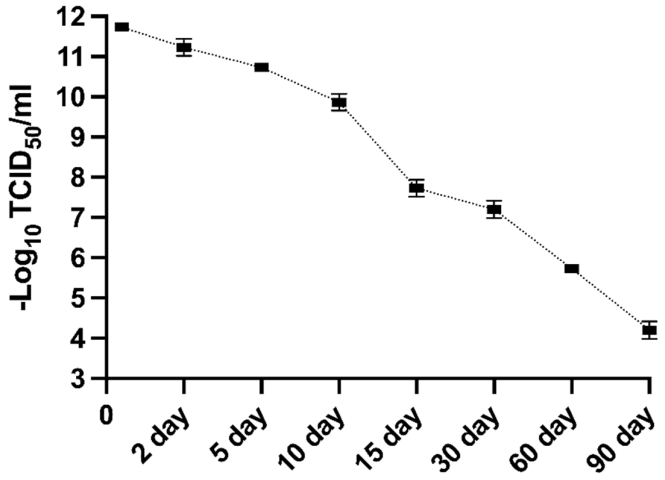

Figure 11. The MFBV suspension was incubated for 90 days, and viral titers were measured at various time points to evaluate the stability of MFBV. Viral titers are expressed as $TCID_{50}$/ml. Each titer value represents the mean ± SE derived from three biological replicates. Partial SE is hidden within the data points.

4. Discussion

In this study, we report the detection and characterization of a novel mandarin fish birnavirus, named MFBV. Furthermore, we validated through Koch's postulates that MFBV is a novel causative agent for mandarin fish. The full-length sequences of MFBV segments A and B were obtained through RACE and molecular cloning and were used for in-depth phylogenetic analyses between MFBV and other RNA viruses. MFBV, LBBV, and LCBV formed a distinct branch with the closest phylogenetic relationship, while other birnaviruses classified by ICTV and newly discovered strains were more distantly related (based on RdRp amino acid sequence analysis: Rocky Mountain birnavirus, 47.94% identity; Wenling jack mackerels birnavirus, 48.05% identity; Wenling Japanese topeshark birnavirus, 50.12% identity).

MFBV VP4 protease and its polyprotein substrate, both exhibit low homology with the other members of the *Birnaviridae* family, raising questions about whether they follow the same cleavage mechanism. To address this, we analyzed the amino acid sequences of MFBV and other birnaviruses VP4 proteins. Alignment of VP4 proteins revealed that the two coordinated amino acids, serine and lysine, are conserved in *Birnaviridae* members. The Ser-Lys catalytic dyad active site in IPNV, IBDV, and BSNV VP4 has been experimentally identified and is considered a serine protease [13,16,22,23], suggesting that MFBV VP4 utilizes a Ser (701)-Lys (738) catalytic dyad (Figure S1A).

Furthermore, we examined the P7-P7' amino acid residues flanking the cleavage sites of MFBV polyprotein. The analysis was based on the cleavage sites of TV-1 polyprotein, which have been experimentally validated [20]. The results revealed that the conserved motif of cleavage site is an alanine (Ala) at position P1 (with the exception of the serine (Ser) in DXV), and no other conserved motifs were found. Additionally, the P1'-P3' sites of the small peptide cleavage sites exhibit conserved ASG amino acid residues, the function of which remains unknown (Figure S1B). These analyses

 doi:10.20944/preprints202412.1420.v1

suggest that although there is significant divergence in birnavirus sequences, the MFBV protease cleavage mechanism is conserved.

RdRp self-guanylylation has been demonstrated in multiple birnaviruses, such as DXV [24], IBDV [25], and IPNV [26]. Specifically, the 5′ ends of the dsRNA genome of birnaviruses are bound to a genome-linked protein (VPg, another form of RdRp) by a Ser-5′-GMP phosphodiester bond at self-guanylylation site [27]. The guanylylation site of IPNV has been determined to be S163 using peptide digestion and site-directed mutagenesis [28]. Additionally, the IBDV guanylylation site residue was putatively identified as S166 [25], and there have been no other analyses of birnaviruses self-guanylylation sites. We used the IPNV guanylylation site amino acid sequence as a reference to predict the guanylylation site in other birnaviruses through homology comparison. Ser residues were found at the corresponding position or at position -2 in all aligned sequences. These residues are also approximately 80 amino acids away from the conserved motif G, suggesting a topological and functional conservation. Based on these findings, we predict S164 as the site for self-guanylylation in MFBV RdRp (Figure S2).

Another feature of the MFBV or other birnaviruses was that RdRp has the unique catalytic core motifs. The prototypic RNA virus RdRp domain harbors seven motifs, which are arranged in the order G, F, A, B, C, D and E from amino- to carboxy-terminus. The only exception to this scheme can be found in some ssRNA (+) non-segmented virus and birnavirus [25,29,30], which is exactly the case with MFBV, it was G-F-C-A-B-D-E. (Figure S3A).

Motifs C and A are the most essential catalytic core motifs in RdRp, housed in the palm subdomain of a right-hand architecture [30–32]. Within motif C, the DD amino acid residues are in the RNA polymerase active site, allowing catalysis to occur via a two-metal mechanism [30,33]. The DD amino acid motif is conserved across most RNA viruses, including positive strand RNA viruses (+RNA), segmented negative strand RNA viruses (seg −RNA), double strand RNA viruses of the reovirus family (Reo dsRNA), and reverse transcriptases (RT). However, the DD amino acid motif is not found in MFBV, instead, it is replaced by the DN motif (Figure S3A). Furthermore, we conducted multiple sequence alignment analysis on representative RdRp sequences from all eleven families within order *Mononegavirales* (negative-sense genome single-stranded RNA viruses, including *Artoviridae, Bornaviridae, Filoviridae, Lispiviridae. Mymonaviridae, Nyamiviridae, Paramyxoviridae, Pneumoviridae, Rhabdoviridae, Sunviridae* and *Xinmoviridae*; ICTV Virus Taxonomy 2023 Release) to examine the conservation of motif C catalytic core. The results indicate that MFBV employs a DN catalytic core consistent with other birnaviruses and *Mononegavirales* viruses (Figure S3A, B) [24,30], for instance, in Ebolavirus [34], respiratory syncytial virus [35], and rabies virus [36]. The DD amino acid residues in RddRp motif C are involved in coordinating interactions with divalent metal ions, which are essential for the phosphoryl transfer reaction [33]. Some suggest that the distinct evolution of the catalytic core in Birnavirus and *Mononegavirales*, from DD to DN, may have enhanced RdRp adaptability to divalent metal ions. The IBDV DN motif has been shown to exhibit greater activity for nucleotide polymerization when utilizing Mn^{2+}, while replaced with DD leads to more efficient coordination with Mg^{2+} [25,37]. However, the DN motif remains a minority in RNA viruses [30]. Whether this feature confers a survival advantage to birnaviruses such as MFBV in natural environments requires further investigation.

Another highly conserved RdRp motif is the DX2-4D amino acid residues in motif A [30,31]. However, in MFBV, this catalytic motif is replaced by DX2K, a pattern unique to segmented negative-strand RNA viruses (seg −RNA) and non-segmented negative-strand RNA (−RNA) viruses [30]. Furthermore, we found that the DX2K motif of MFBV is completely consistent with that of most birnaviruses and the family *Filoviridae* of order *Mononegavirales*, specifically DLEK motif. This family includes well-known viruses such as Ebola virus and Marburg virus, as well as fish filoviruses discovered through virus metagenomic studies (Wenling frogfish filovirus strain, MG599980.1; Wenling thamnaconus septentrionalis filovirus, MG599981.1). Both the DN and DLEK catalytic motifs are rare among RNA viruses, the concurrent utilization of these two motifs by both birnaviruses and filoviruses may suggest a potential evolutionary relationship between the two (Figure S3A,B). However, based on capsid topology analysis, the jelly roll structure of IBDV VP2

 doi:10.20944/preprints202412.1420.v1

(within segment A) and its inserted domain were respectively linked to two different categories of RNA viruses: Black Beetle virus (Nodaviridae, non-enveloped positive-strand RNA viruses, T=3) and rotavirus (Reoviridae, non-enveloped double-stranded RNA viruses, external and intermediate layer, T=13) [21]. Along with our discovery of the phylogenetic relationship between segment B and filoviruses in this study, this supports the hypothesis that birnavirus segments A and B have undergone reassortment and followed distinct evolutionary pathways [14,38].

The untranslated regions (UTRs)of birnavirus genome are essential for replication and translation processes [37,39]. The 5'UTR serves as a binding site for VPg [40,41] and the 3'UTR cytosines allow protein-primed initiation of second strand RNA synthesis [26,37]. The precise sequences of 5'UTR and 3'UTR have been experimentally determined for some birnaviruses, such as LBBV [6], BSNV [13], IPNV [11], IBDV [12] and TV-1 [20]. Multiple sequence alignment analysis of MFBV and these birnaviruses revealed a conserved starting motif of GGAAA (except for IBDV's GGAUA) (Figure S4). Additionally, the two constitutive cytosines at 3' terminus (except for LBBV and TV-1 segment B) form a small stem-loop secondary structure, which is crucial for virus replication or virulence [42]. However, the position and length of the 3'UTR stem-loop end are not fixed in birnaviruses (Figure S4).

Birnavirus mRNA is known to lack a cap, thus relying on cap-independent mechanisms for translation initiation. However, the relatively short 5'UTR of birnaviruses appears insufficient to form a typical internal ribosome entry site (IRES) for translation initiation (a cap-independent mechanism) [42]. While there are reports of IPNV segment A having IRES within the 120bp 5'UTR [43], whether this critical IRES secondary structure is conserved in MFBV remains unknown. We used MXfold2 (http://www.dna.bio.keio.ac.jp/mxfold2/) [44] to predict the MFBV 5'UTR secondary structure. The result revealed the stem-loop structures at the 5' ends of segments A and B of MFBV, albeit simpler compared to known IRES structures of four classes [45,46]. Furthermore, MFBV's segment A 5'UTR is only 170 bp, and segment B 5'UTR is only 96 bp, significantly shorter than compact typical Class III (332 bp) [45,47] or Class IV intergenic region IRES (191 bp, KP974706.1) structures [45]. Therefore, it is speculated that IRES may not be universally present in birnaviruses, at least not in MFBV, suggesting that MFBV may initiate translation through alternative pathways (Figure S5).

For IPNV, the complete replication cycle takes about 24 hours at 15°C, but is shortened to 16-20 hours at 22°C in salmon embryo (CHSE-214) cells, with replication ceasing at 28°C [48–50]. MFBV exhibits a replication cycle of 8-10 hours at 27°C in SCK cells. At their respective suitable replication temperatures, MFBV replicates significantly faster than IPNV. Furthermore, approximately $10^{7.9}$ MFBV RNA copies per μg total RNA can be detected in the spleen as early as 16 hpi, which means MFBV replication is also notably faster than other pathogens of mandarin fish, such as ISKNV [51] and MRV [8]. The rapid replication kinetics may explain why severe symptoms, including mortality, occur as early as 6 hours post-infection in mandarin fish. In contrast, other mandarin fish viral pathogens such as ISKNV and MRV typically require 3-5 days to induce mortality even at high inoculum doses [8,51]. Further, in all fourteen tissues, the MFBV RNA copies per μg total RNA exceeded $10^{6.9}$, with only a tenfold difference between the tissue with the highest (spleen) and the lowest (gonad). This suggests that MFBV does not show significant tissue tropism and is capable of causing systemic multi-organ infections. It is speculated that severe systemic infection is another factor contributing to the rapid mortality. Additionally, it is noteworthy that the threat of MFBV to fry is greater than that to juveniles, as evidenced by the higher mortality rate of fry (approximately 30%-40% higher). This corresponds to the birnavirus outbreak in a mandarin fish fry factory in Yangchun City in May 2023, when millions of week-old fry died within 48 hours, with a mortality rate of nearly 100%.

To mitigate MFBV outbreaks, we tested its sensitivity to various disinfectants. The experimental concentration ranges of disinfectants in this study were determined based on the study on ISKNV, and *Micropterus salmoides* rhabdovirus. ISKNV can be inactivated by sodium hypochlorite (1000 ppm for 30 minutes) and benzalkonium chloride (650 ppm for 10 minutes) [52] , while *M. salmoides* rhabdovirus can be inactivated by 500 ppm povidone-iodine and 500 ppm glutaraldehyde within 30 minutes [53]. Based on these results presented, one or more disinfectants can be chosen for different

 doi:10.20944/preprints202412.1420.v1

epidemic outbreaks. Additionally, in the laboratory, a 15-day storage reduced MFBV infectivity by 99.9%, suggesting natural decay could be an alternative in the absence of disinfection. However, organic and inorganic substances in natural water may affect decay rates [54], requiring further optimization.

Taken together, this research may have important implications for exploring the MFBV replication mechanism and developing disease containment strategies.

Supplementary Materials: The following supporting information can be downloaded at: www.mdpi.com/xxx/s1, Figure S1. (A) The catalytic dyad of VP4. The amino acid sequence of VP4 was aligned using Kalign. IPNV, IBDV, and BSNV VP4 served as reference for homology comparison to predict the catalytic site of MFBV VP4. The catalytic dyad of VP4 is highlighted in orange. (B) The conserved amino acid residues of polyprotein cleavage sites. Scissors indicate the predicted cleavage sites of the MFBV polyprotein. The conserved amino acid is indicated below. Completely conserved sites are highlighted in orange, positions with two types of amino acids are shown in yellow, and positions with three amino acids are highlighted in green. Figure S2. Guanylylation sites of MFBV and other birnaviruses are highlighted in orange, predicted based on homology alignment with the guanylylation site of IPNV RdRp. Figure S3. (A)Key conserved residues of the RdRp motifs. The RdRp amino acid sequence was of aligned using Kalign, the numbers indicating the positions of the motifs. Completely conserved sites are highlighted in orange, positions with two types of amino acids are highlighted in yellow, and positions with three amino acids are shown in green. (B) Comparison of catalytic core amino acids in motifs A and C between birnaviruses and Mononegavirales viruses. The data include representative viruses from all 11 families of the order Mononegavirales and representative viruses from 7 genera of the Filoviridae family. Completely conserved sites between Mononegavirales viruses and birnaviruses are highlighted in orange, residues conserved only within each set are highlighted in yellow. The sequence identifiers are arranged as family, genus, strain and accession number. If there is no genus, then only the strain name is displayed. Figure S4. UTR sequences of birnaviruses. Conserved motifs are highlighted in orange. Figure S5. Secondary structure prediction of birnavirus UTRs. The data includes only virus UTR sequences that have been determined through experimental methods.

Author Contributions: Conceptualization, H.Z.; Methodology, H.Z., D.Z., Y.Y. and S.L.; Resources, H.Z., J.D. and J.H.; Writing—original draft, H.Z.; Writing—review & editing, H.Z., J.H., D.Z., S.L., X.Y., J.D. and C.S.; Funding acquisition, X.Y. and C.S. All authors have read and agreed to the published version of the manuscript.

Funding: This research was funded by National Key R&D Program of China, grant number 2023YFD2402900, Key-Area Research and Development Program of Guangdong Province, grant number 2021B0202020001; China Agriculture Research System of MOF and MARA, grant number CARS-46; Central Public-interest Scientific Institution Basal Research Fund, grant numbers CAFS, PRFRI-CAFS; Rural Revitalization Strategic Special Funds Provincial Projects, grant number 2021.

Institutional Review Board Statement: The animal study protocol was approved by the Institutional Review Board of the Pearl River Fisheries Research Institute, Chinese Academy of Fishery Sciences (LAEC-PRFRI-2023-05-20).

Data Availability Statement: The cell lines metadata presented in this study are openly available in the NCBI BioSample database. SCK cell line: [Accession Number: SAMN38845202] (Link: https://www.ncbi.nlm.nih.gov/biosample/38845202); The MFBV genome accession numbers are PP786692.1 and PP786693.1.

Acknowledgments: We thank Jian He from Sun Yat-sen University for his valuable suggestions on the manuscript.

Conflicts of Interest: The authors declare no conflict of interest.

References

1. Hjalmarsson A, Carlemalm E, Everitt E. Infectious pancreatic necrosis virus: identification of a VP3-containing ribonucleoprotein core structure and evidence for O-linked glycosylation of the capsid protein VP2. *J Virol. 1999.* 73:3484-90
2. Brodrick AJ, Broadbent AJ. The Formation and Function of Birnaviridae Virus Factories. *Int J Mol Sci. 2023.* 24
3. Luque D, Rivas G, Alfonso C, Carrascosa JL, Rodriguez JF, Caston JR. Infectious bursal disease virus is an icosahedral polyploid dsRNA virus. *Proc Natl Acad Sci U S A. 2009.* 106:2148-52
4. Villanueva RA, Galaz JL, Valdes JA, Jashes MM, Sandino AM. Genome assembly and particle maturation of the birnavirus infectious pancreatic necrosis virus. *J Virol. 2004.* 78:13829-38

5. Chen J, Toh X, Ong J, Wang Y, Teo XH, et al. Detection and characterization of a novel marine birnavirus isolated from Asian seabass in Singapore. *Virol J. 2019.* 16:71
6. Fu X, Luo M, Zheng G, Liang H, Liu L, et al. Determination and Characterization of a Novel Birnavirus Associated with Massive Mortality in Largemouth Bass. *Microbiol Spectr. 2022.* 10:e0171621
7. Shi M, Lin XD, Chen X, Tian JH, Chen LJ, et al. The evolutionary history of vertebrate RNA viruses. *Nature. 2018.* 556:197-202
8. Zhang H, Dong J, Yan Y, Liu S, Ye X, et al. Development of a Highly Permissive Mandarin Fish (Siniperca chuatsi) Kidney Cell Line for Mandarin Fish Ranavirus Using a Single-Cell Cloning Method. *Cells. 2023.* 13
9. Lassmann T, Sonnhammer EL. Kalign--an accurate and fast multiple sequence alignment algorithm. *BMC Bioinformatics. 2005.* 6:298
10. Wulff NH, Tzatzaris M, Young PJ. Monte Carlo simulation of the Spearman-Kaerber TCID50. *J Clin Bioinforma. 2012.* 2:5
11. Dobos P. The molecular biology of infectious pancreatic necrosis virus (IPNV). *Annual Review of Fish Diseases. 1995.* 5:25-54
12. Hudson PJ, McKern NM, Power BE, Azad AA. Genomic structure of tbe large RNA segment of infectious bursal disease virus. *Nucleic acids research. 1986.* 14:5001-12
13. Da Costa B, Soignier S, Chevalier C, Henry C, Thory C, et al. Blotched snakehead virus is a new aquatic birnavirus that is slightly more related to avibirnavirus than to aquabirnavirus. *J Virol. 2003.* 77:719-25
14. Gibrat JF, Mariadassou M, Boudinot P, Delmas B. Analyses of the radiation of birnaviruses from diverse host phyla and of their evolutionary affinities with other double-stranded RNA and positive strand RNA viruses using robust structure-based multiple sequence alignments and advanced phylogenetic methods. *BMC Evol Biol. 2013.* 13:154
15. Mundt E, Beyer J, Muller H. Identification of a novel viral protein in infectious bursal disease virus-infected cells. *J Gen Virol. 1995.* 76 (Pt 2):437-43
16. Petit S, Lejal N, Huet JC, Delmas B. Active residues and viral substrate cleavage sites of the protease of the birnavirus infectious pancreatic necrosis virus. *J Virol. 2000.* 74:2057-66
17. Chung HK, Kordyban S, Cameron L, Dobos P. Sequence analysis of the bicistronic Drosophila X virus genome segment A and its encoded polypeptides. *Virology. 1996.* 225:359-68
18. Wu Q, Luo Y, Lu R, Lau N, Lai EC, et al. Virus discovery by deep sequencing and assembly of virus-derived small silencing RNAs. *Proc Natl Acad Sci U S A. 2010.* 107:1606-11
19. Galloux M, Libersou S, Morellet N, Bouaziz S, Da Costa B, et al. Infectious bursal disease virus, a non-enveloped virus, possesses a capsid-associated peptide that deforms and perforates biological membranes. *J Biol Chem. 2007.* 282:20774-84
20. Nobiron I, Galloux M, Henry C, Torhy C, Boudinot P, et al. Genome and polypeptides characterization of Tellina virus 1 reveals a fifth genetic cluster in the Birnaviridae family. *Virology. 2008.* 371:350-61
21. Coulibaly F, Chevalier C, Gutsche I, Pous J, Navaza J, et al. The birnavirus crystal structure reveals structural relationships among icosahedral viruses. *Cell. 2005.* 120:761-72
22. Lejal N, Da Costa B, Huet JC, Delmas B. Role of Ser-652 and Lys-692 in the protease activity of infectious bursal disease virus VP4 and identification of its substrate cleavage sites. *J Gen Virol. 2000.* 81:983-92
23. Birghan C, Mundt E, Gorbalenya AE. A non-canonical lon proteinase lacking the ATPase domain employs the ser-Lys catalytic dyad to exercise broad control over the life cycle of a double-stranded RNA virus. *EMBO J. 2000.* 19:114-23
24. Shwed PS, Dobos P, Cameron LA, Vakharia VN, Duncan R. Birnavirus VP1 proteins form a distinct subgroup of RNA-dependent RNA polymerases lacking a GDD motif. *Virology. 2002.* 296:241-50
25. Pan J, Vakharia VN, Tao YJ. The structure of a birnavirus polymerase reveals a distinct active site topology. *Proc Natl Acad Sci U S A. 2007.* 104:7385-90
26. Dobos P. In vitro guanylylation of infectious pancreatic necrosis virus polypeptide VP1. *Virology. 1993.* 193:403-13
27. Calvert JG, Nagy E, Soler M, Dobos P. Characterization of the VPg-dsRNA linkage of infectious pancreatic necrosis virus. *J Gen Virol. 1991.* 72 (Pt 10):2563-7
28. Xu HT, Si WD, Dobos P. Mapping the site of guanylylation on VP1, the protein primer for infectious pancreatic necrosis virus RNA synthesis. *Virology. 2004.* 322:199-210
29. Gorbalenya AE, Pringle FM, Zeddam JL, Luke BT, Cameron CE, et al. The palm subdomain-based active site is internally permuted in viral RNA-dependent RNA polymerases of an ancient lineage. *J Mol Biol. 2002.* 324:47-62
30. te Velthuis AJ. Common and unique features of viral RNA-dependent polymerases. *Cell Mol Life Sci. 2014.* 71:4403-20
31. Venkataraman S, Prasad B, Selvarajan R. RNA Dependent RNA Polymerases: Insights from Structure, Function and Evolution. *Viruses. 2018.* 10
32. Jacome R, Becerra A, Ponce de Leon S, Lazcano A. Structural Analysis of Monomeric RNA-Dependent Polymerases: Evolutionary and Therapeutic Implications. *PLoS One. 2015.* 10:e0139001

33. Gong P, Peersen OB. Structural basis for active site closure by the poliovirus RNA-dependent RNA polymerase. *Proc Natl Acad Sci U S A. 2010.* 107:22505-10
34. Hume AJ, Muhlberger E. Distinct Genome Replication and Transcription Strategies within the Growing Filovirus Family. *J Mol Biol. 2019.* 431:4290-320
35. Gilman MSA, Liu C, Fung A, Behera I, Jordan P, et al. Structure of the Respiratory Syncytial Virus Polymerase Complex. *Cell. 2019.* 179:193-204 e14
36. Horwitz JA, Jenni S, Harrison SC, Whelan SPJ. Structure of a rabies virus polymerase complex from electron cryo-microscopy. *Proc Natl Acad Sci U S A. 2020.* 117:2099-107
37. von Einem UI, Gorbalenya AE, Schirrmeier H, Behrens SE, Letzel T, Mundt E. VP1 of infectious bursal disease virus is an RNA-dependent RNA polymerase. *J Gen Virol. 2004.* 85:2221-9
38. Romero-Brey I, Bandin I, Cutrin JM, Vakharia VN, Dopazo CP. Genetic analysis of aquabirnaviruses isolated from wild fish reveals occurrence of natural reassortment of infectious pancreatic necrosis virus. *J Fish Dis. 2009.* 32:585-95
39. Ye C, Wang Y, Zhang E, Han X, Yu Z, Liu H. VP1 and VP3 Are Required and Sufficient for Translation Initiation of Uncapped Infectious Bursal Disease Virus Genomic Double-Stranded RNA. *J Virol. 2018.* 92
40. Magyar G, Chung HK, Dobos P. Conversion of VP1 to VPg in cells infected by infectious pancreatic necrosis virus. *Virology. 1998.* 245:142-50
41. Gonzalez-Catrilelbun S, Cartagena J, Vargas D, Breguel-Serrano P, Sandino AM, Rivas-Aravena A. The RNA-dependent RNA polymerase of the infectious pancreatic necrosis virus is linked to viral mRNA acting as a cap substitute. *J Gen Virol. 2022.* 103
42. Boot HJ, Pritz-Verschuren SB. Modifications of the 3'-UTR stem-loop of infectious bursal disease virus are allowed without influencing replication or virulence. *Nucleic Acids Res. 2004.* 32:211-22
43. Rivas-Aravena A, Munoz P, Jorquera P, Diaz A, Reinoso C, et al. Study of RNA-A Initiation Translation of The Infectious Pancreatic Necrosis Virus. *Virus Res. 2017.* 240:121-9
44. Sato K, Akiyama M, Sakakibara Y. RNA secondary structure prediction using deep learning with thermodynamic integration. *Nat Commun. 2021.* 12:941
45. Mailliot J, Martin F. Viral internal ribosomal entry sites: four classes for one goal. *Wiley Interdiscip Rev RNA. 2018.* 9
46. Lee KM, Chen CJ, Shih SR. Regulation Mechanisms of Viral IRES-Driven Translation. *Trends Microbiol. 2017.* 25:546-61
47. Spahn CM, Kieft JS, Grassucci RA, Penczek PA, Zhou K, et al. Hepatitis C virus IRES RNA-induced changes in the conformation of the 40s ribosomal subunit. *Science. 2001.* 291:1959-62
48. Dopazo CP. The Infectious Pancreatic Necrosis Virus (IPNV) and its Virulence Determinants: What is Known and What Should be Known. *Pathogens. 2020.* 9
49. Lannan CN, Winton JR, Fryer JL. Fish cell lines: establishment and characterization of nine cell lines from salmonids. *In Vitro. 1984.* 20:671-6
50. Roberts TE, Dobos P. Studies on the mechanism of temperature sensitivity of infectious pancreatic necrosis virus replication. *J Gen Virol. 1983.* 64 (Pt 2):331-9
51. Zhang H, Qi H, Weng S, He J, Dong C. Deleting ORF71L of infectious spleen and kidney necrosis virus (ISKNV) resulted in virulence attenuation in Mandarin fi sh. *Fish Shellfish Immunol. 2022.* 123:335-47
52. Fusianto C, Hick PM, Becker JA. Stability of Infectious spleen and kidney necrosis virus and susceptibility to physical and chemical disinfectants. *Aquaculture. 2019.* 506:104-11
53. He R, Zhu N, Chen X, Liang Q, Yao G, et al. Experimental evidence of effective disinfectant to control the transmission of Micropterus salmoides rhabdovirus. *J Fish Dis. 2024.* 47:e13891
54. Oidtmann B, Dixon P, Way K, Joiner C, Bayley AE. Risk of waterborne virus spread–review of survival of relevant fish and crustacean viruses in the aquatic environment and implications for control measures. *Reviews in aquaculture. 2018.* 10:641-69